

Logic gates and optical switching with vertical-cavity surface-emitting lasers

F. Prati,* M. Travagnin, and L. A. Lugiato

*Dipartimento di Fisica dell' Università di Milano, via Celoria 16, 20133 Milano, Italy
and Istituto Nazionale per la Fisica della Materia, via Celoria 16, 20133 Milano, Italy*

(Received 11 December 1995)

We show that an index—and gain—guided vertical-cavity surface-emitting laser with a square-shaped active region can operate as a bistable laser with the two Gauss-Hermite modes TEM_{10} and TEM_{01} . Optical switching from one mode to the other upon injection of appropriate Gaussian pulses is numerically investigated; the switching energy can be as small as 30 fJ and the process is completed in a time of the order of a few nanoseconds. We demonstrate the possibility of using the laser as a logic gate of the NOR, OR, NOT type. Carrier diffusion increases laser threshold and the size of the bistability domain, and it reduces both switching time and switching energy. [S1050-2947(96)06812-6]

PACS number(s): 42.65.Pc, 42.79.Ta

I. INTRODUCTION

The last decade witnessed the development of the field of transverse nonlinear optics [1,2], which studies the phenomena of spontaneous pattern formation and transformation which occur in the structure of the electric field in the planes orthogonal to the direction of propagation, when the radiation interacts with nonlinear optical media. Spontaneous pattern formation in nonlinear optics has been demonstrated in Kerr systems [3], in lasers [4], in photorefractive oscillators [5], in liquid crystals [6], in liquid-crystals-light valves (LCLV) [7], and in atomic vapors [8]. A more complete list of references can be found in [9].

The fast time evolution in optical systems makes transverse nonlinear optics potentially useful for applications to information processing. In this perspective the phenomenon of “spatial multistability” is of great relevance [10,11]. It consists in the capability, displayed by several kinds of lasers, of emitting beams with different spatial configurations, under the same parametric conditions. This situation is quite different from standard optical bistability, where the stable states differ only for the emitted power. On the contrary, in spatial multistability the total emitted power for the different stable states is usually almost the same. The different states can be distinguished only on the basis of the field spatial configuration.

The simplest case of multistability is represented by bistability of the two lowest-order doughnut modes, which has been experimentally demonstrated in a He–Ne laser [12]. Application to optical switching has been reported in [13], where it has been shown that the bistable laser can switch from one to the other doughnut mode by injection of an external field whose intensity is very small, compared with that of the slave laser.

Our first aim, when we started working on this research, was to simply extend the results of [13] to a class of lasers such as VCSELs (vertical-cavity surface-emitting lasers) [14] which are much more suitable for practical applications, because of their small dimensions and fast response.

Yet, even the crudest attempt to model transverse effects in VCSELs, which consists in a rate equation model which takes into account the band structure of the energy levels by means of the introduction of the phenomenological linewidth enhancement factor α [15], showed that the behavior of VCSELs is very different from that of gas lasers, which can be described by the standard Maxwell-Bloch equations for two-level atoms.

It is known that in class-A lasers, and in class-B lasers under conditions of resonance between the gain line and the cavity, the doughnut modes are always stable for every choice of the parameters [18]. In the simple model of [16] VCSELs turn out to be mathematically equivalent to class-B lasers with a normalized atomic detuning equal to α . Since α ranges normally from 3 to 6 [15], the correspondence is with class-B lasers with large atomic detuning. For this kind of laser the doughnut modes are unstable almost everywhere and the most common situation is that in which the laser develops undamped oscillations. However, for $\alpha > 1$ a stability domain for modes TEM_{10} and TEM_{01} exists in the parameter space [16].

The latter result was quite surprising, because previously it was believed that modes TEM_{10} or TEM_{01} could be stabilized only by a breaking of the cylindrical symmetry [19] which favors one of the two. Therefore bistability between these two modes was excluded *a priori*. In VCSELs, instead, it is possible to obtain bistability between TEM_{10} and TEM_{01} by considering an active region of a square instead of a circular section [16].

From the point of view of applications this kind of bistability is even preferable to bistability between doughnut modes, because it allows us to obtain switching using Gaussian-shaped control beams, and to realize logic gates. These are precisely the issues that we want to analyze in this paper. A sketchy account of this research was provided in [17]; here we give a detailed discussion of the physical assumptions and a complete description of the analytical and numerical treatment. In addition, we introduce a necessary completion of our model by including also carrier diffusion in the transverse plane.

In Sec. II we introduce the model for an index—and

*FAX: +39-2-2392712; Electronic address: prati@milano.infn.it

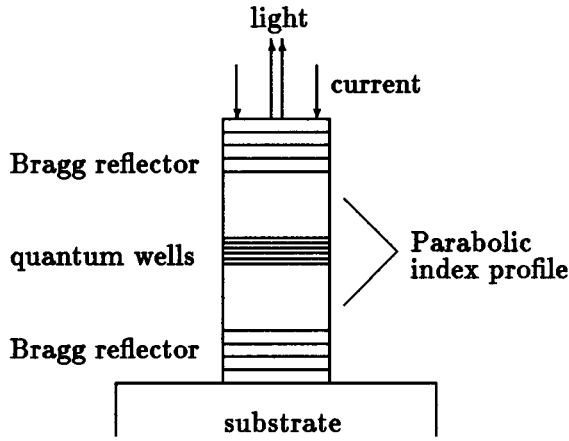


FIG. 1. Schematic representation of the laser.

gain—guided VCSEL and in Sec. III we summarize the analytical results obtained in [16]. Numerical simulations of optical switching of modes TEM_{10} and TEM_{01} are presented in Sec. IV, where the essential role of detuning between the injecting laser and the slave laser is also discussed. In Sec. V we suggest a scheme for the realization of NOR, OR, and NOT gates based on the bistable VCSEL. The effects of carrier diffusion are discussed in Sec. VI. Section VII is devoted to the concluding remarks and to the discussion of the limits of the model.

II. THE MODEL

Let us consider the VCSEL schematically represented in Fig. 1. The Cartesian reference frame (x, y, z) is oriented in such a way that light propagates along z . L is the length of the cavity, considering the penetration inside the Bragg reflectors with reflectivity R and transmissivity $T = 1 - R$; L_A is the thickness of the active region and S is the cross section of the laser, whose actual shape is not important because we will assume that the cross section of the active region is much smaller than laser cross section. Typical values are $L \approx 2 \mu\text{m}$, $L_A \approx 0.05 \mu\text{m}$, $S \approx 100 \mu\text{m}^2$, and $R > 0.99$. If the active material is GaAs, the wavelength inside the material is $\lambda \approx 0.24 \mu\text{m}$. Thus, the cavity volume $V = SL \approx 200 \mu\text{m}^3$ is much larger than λ^3 , and microcavity effects, such as the influence of spontaneous emission on lasing threshold, can be neglected.

Because of their geometry VCSEL's, unlike conventional edge-emitting semiconductor lasers, are able to emit Gauss-Laguerre or Gauss-Hermite modes, as reported in several experiments [20–26]. The spatial profile and frequency spectrum of the observed modes is not different from that of a conventional Fabry-Pèrot laser with spherical mirrors in the near planar configuration (transverse frequency spacing much smaller than longitudinal frequency spacing). In a Fabry-Pèrot resonator the wave-front curvature of Gaussian modes is induced by spherical mirrors. In a VCSEL mirrors are replaced by Bragg reflectors and the wave-front curvature can be explained in terms of variations of the refractive index in the transverse plane, due to thermal gradients. The refractive index on laser axis, where the temperature is higher, is

larger than on the edge. Thus any VCSEL is unavoidably weakly index guiding.

We model weak index guiding assuming that, independently of the modes which are activated, the refractive index has a parabolic profile in the transverse plane

$$n^2(x, y) = n_0^2 \left(1 - \frac{x^2 + y^2}{h^2} \right), \quad (2.1)$$

with h much larger than the transverse dimension of the laser, in such a way that the variation of the refractive index from axis to edge is small. We have chosen a parabolic profile among all the possible ones because with this choice Gaussian modes are exact solutions of the paraxial wave. A different choice would only introduce big mathematical difficulties, but no relevant physical differences. Gauss-Hermite modes are labeled by the indices m and n and they are described by the functions [16]

$$\mathcal{A}_{mn}(x, y, z) = A_{mn}(x, y) \exp \left[-i(m+n+1) \frac{z}{h} \right], \quad (2.2a)$$

$$A_{mn}(x, y) = \frac{N_{mn}}{w_0} \exp \left[-\frac{x^2 + y^2}{w_0^2} \right] H_m \left(\sqrt{2} \frac{x}{w_0} \right) H_n \left(\sqrt{2} \frac{y}{w_0} \right), \quad (2.2b)$$

where $N_{mn} = (\pi m! n! 2^{m+n-1})^{-1/2}$ is a normalization term. The beam waist w_0 of the fundamental Gaussian mode TEM_{00} is related to the index-guiding parameter h and to the wavelength λ inside the material by Eq. [16]

$$w_0 = \left(\frac{\lambda h}{\pi} \right)^{1/2}. \quad (2.3)$$

Therefore h plays the same role as the Rayleigh length in an open resonator with spherical mirrors. The frequency of mode (m, n) is

$$\omega_{qmn} = \frac{c}{n_0 L} \left[\pi q + \frac{L}{h} (m+n+1) \right], \quad (2.4)$$

where q is the longitudinal index. Modes with the same value of $m+n$ but different values of m and n are degenerate in frequency. According to Eq. (2.4) the transverse frequency spacing is

$$\Delta \omega_T = \frac{c}{h n_0}. \quad (2.5)$$

Equations (2.3) and (2.5) give two independent estimates of the unknown index-guiding parameter h . Their self-consistency is a check of the validity of the model. For instance, by putting $w_0 = 3 \mu\text{m}$ and $\lambda = 0.24 \mu\text{m}$ in Eq. (2.3) we obtain $h \approx 117 \mu\text{m}$, which, substituted in Eq. (2.5) with $n_0 = 3.5$, yields $\Delta \omega_T / (2\pi) \approx 117 \text{ GHz}$, in agreement with reported values. Note that $h^2 \gg S$ is in agreement with our initial assumptions.

The very short cavity length of a VCSEL implies that in this kind of laser only one longitudinal mode is active. Thus, we can safely introduce in our model the single longitudinal mode approximation. On the other hand, the very high reflectivities and the smallness of the active region ensure the

validity of the mean-field limit, in which the dependence on the longitudinal coordinate z can be neglected and the forward and backward fields have the same value. Note that this assumption is often made also for edge-emitting lasers, even if in that case it is less justified, because the reflectivities are much smaller than 1.

We consider then a single electric field with a slowly varying envelope $F(x,y,t)$ and expand it in terms of the modes $A_{mn}(x,y)$

$$F(x,y,t) = \sum_{mn} A_{mn}(x,y) f_{mn}(t). \quad (2.6)$$

The other dynamical variable is the appropriately renormalized carrier density

$$D(x,y,t) = \frac{aL_A}{T} [N(x,y,t) - N_0], \quad (2.7)$$

where $N(x,y,t)$ is the total carrier density, N_0 the transparency value ($N_0 \approx 2 \times 10^{18} \text{ cm}^{-3}$), a the gain coefficient ($a \approx 3 \times 10^{-16} \text{ cm}^2$). The complex mode amplitudes f_{mn} and carrier density D obey the amplitude rate equations [16]

$$\begin{aligned} \frac{df_{mn}}{dt} = & -\frac{1}{\tau_p} \left[(1 + ia_{mn}) f_{mn} - (1 - i\alpha) \right. \\ & \left. \times \int_{-\infty}^{\infty} dx \int_{-\infty}^{\infty} dy A_{mn} D F \right], \end{aligned} \quad (2.8a)$$

$$\frac{\partial D}{\partial t} = -\frac{1}{\tau_r} [D(1 + |F|^2) - \chi(x,y) - l_D^2 \nabla_{\perp}^2 D]. \quad (2.8b)$$

In the last equation we neglected both diffusion and grating in the longitudinal direction, assuming that the effect of longitudinal diffusion is just to wash up any grating in the longitudinal profile of carrier density.

It must be noted that in real devices the active region consists of a small number of quantum wells and diffusion can act only inside the single well. Therefore the longitudinal profile of carrier density is constant in the single well but it assumes, in general, different values for each well. To avoid this complication we consider a single quantum well or, equivalently, we neglect this variation assuming that the profile of a carrier density is constant along the whole active region. This is consistent with the assumptions of a uniform field model.

On the other hand, we took into account diffusion in the transverse plane; l_D is the diffusion length. In other words, we say that $L_A \ll l_D \ll w_0$, with $L_A \approx 0.05 \mu\text{m}$ and $w_0 \approx 3 \mu\text{m}$. The time scales of the dynamical system (2.8a) are the photon lifetime

$$\tau_p = \frac{2n_0 L}{cT} \quad (2.9)$$

and the recombination time τ_r . If we set $n_0 = 3.5$, $L = 2 \mu\text{m}$ and $T = 0.0025$, we obtain $\tau_p \approx 20$ ps. The recombination time, which is usually taken as 1 ns, is known to become smaller when laser action starts, reaching values as small as 0.2 ns [27]. Thus, the ratio τ_p / τ_r in a VCSEL with very high

reflectivities may be as large as 0.1, two orders of magnitude larger than in a conventional edge-emitting laser.

The other parameters are the linewidth enhancement factor α and the transverse frequency spacing between mode (m,n) and the fundamental Gaussian mode

$$a_{mn} = (\omega_{qmn} - \omega_{q00}) \tau_p. \quad (2.10)$$

In a gain-guided VCSEL, the injected current is confined in the transverse direction, usually by ion implantation. The cross section of the active region is smaller than the cross section of the laser. This feature is represented in our model by the function $\chi(x,y)$, which is the normalized transverse profile of the injected current

$$\chi(x,y) = \frac{aL_A N_0}{T} \left[\frac{I(x,y)}{I_0} - 1 \right]. \quad (2.11)$$

I_0 is the current necessary to achieve transparency and it is related to the transparency carrier density N_0 by the equation

$$I_0 = \frac{q_e V N_0}{\tau_r}, \quad (2.12)$$

where q_e is the electron charge.

We consider the case in which the cross section of the active region is a square of size l_A . The injected current is equal to a certain value $I > I_0$ inside the square and it vanishes outside. Then, the function χ is

$$\chi = \begin{cases} \mu = \frac{aL_A N_0}{T} \left[\frac{I}{I_0} - 1 \right], & |x|, |y| \leq l_A/2, \\ \mu_0 = -\frac{aL_A N_0}{T}, & |x|, |y| > l_A/2. \end{cases} \quad (2.13)$$

The term μ_0 represents absorption in that part of the quantum well which is not traversed by the injected current. However, we have set $\mu_0 = 0$, while keeping $\mu \neq 0$. In this way we neglect absorption in the quantum well as well as we neglect it in the region between the quantum well and the Bragg reflectors. This assumption allows us to simplify the analytic calculations, without changing significantly the final results. Actually, the main effect of absorption is to increase the laser threshold μ_{thr} , but this is quite irrelevant, since we express our results in terms of the ratio μ / μ_{thr} which is independent of the actual value μ_{thr} . We will again discuss this point in the final section.

For $\mu_0 = 0$ our adimensional laser threshold μ_{thr} is related to the threshold current I_{thr} by the equation

$$I_{thr} = I_0 \left[1 + \frac{T}{aL_A N_0} \mu_{thr} \right]. \quad (2.14)$$

The particular value of μ_{thr} depends on the laser geometry and on the shape of the active modes, as is shown in Sec. III.

III. STABILITY DOMAINS OF STATIONARY SOLUTIONS NEGLECTING CARRIER DIFFUSION

We are interested in the case in which only the two modes A_{10} and A_{01} belonging to the frequency degenerate family $m+n=1$ are active. This condition can be obtained by put-

ting a small absorbing or metallic dot on the laser axis to suppress the fundamental Gaussian mode TEM_{00} and a window of appropriate size on the top surface to cut the higher-order modes. We take as a reference frequency the common frequency of family $m+n=1$ properly pulled by the quantity α/τ_p . The dynamical equations of the laser, neglecting diffusion ($l_D=0$), are then

$$\frac{df_{10}}{dt} = -\frac{1}{\tau_p}(1-i\alpha)\left[f_{10} - \int_{-\infty}^{\infty} dx \int_{-\infty}^{\infty} dy A_{10} DF\right], \quad (3.1a)$$

$$\frac{df_{01}}{dt} = -\frac{1}{\tau_p}(1-i\alpha)\left[f_{01} - \int_{-\infty}^{\infty} dx \int_{-\infty}^{\infty} dy A_{01} DF\right], \quad (3.1b)$$

$$\frac{\partial D}{\partial t} = -\frac{1}{\tau_r}[D(1+|F|^2) - \chi(x,y)], \quad (3.1c)$$

with

$$F(x,y,t) = A_{10}(x,y)f_{10}(t) + A_{01}(x,y)f_{01}(t) \quad (3.2)$$

and

$$A_{10}(x,y) = \left(\frac{2}{\pi}\right)^{1/2} \frac{2x}{w_0^2} \exp\left[-\frac{x^2+y^2}{w_0^2}\right], \quad (3.3a)$$

$$A_{01}(x,y) = \left(\frac{2}{\pi}\right)^{1/2} \frac{2y}{w_0^2} \exp\left[-\frac{x^2+y^2}{w_0^2}\right]. \quad (3.3b)$$

The stationary solutions of Eqs. (3.1) are obtained by setting the time derivatives equal to zero. One has in general

$$F^{st}(x,y) = A_{10}(x,y)f_{10}^{st} + A_{01}(x,y)f_{01}^{st}. \quad (3.4)$$

As shown in [16] there are three kinds of stationary solutions: (a) The pure modes A_{10} ($f_{01}^{st}=0$) and A_{01} ($f_{10}^{st}=0$) with nodal lines coincident, respectively, with the y axis and the x axis. (b) The same modes rotated by $\pi/4$, in such a way that the nodal lines coincide with the diagonals of the pumped square. The mode amplitudes are such that $f_{10}^{st}=f^{st}$, $f_{01}^{st}=\pm f^{st}$. The stationary field can then be written as $F^{st}=B_{1,2}f^{st}$ where the modes B_1 and B_2 are defined as

$$B_1(x,y) = \frac{A_{10}+A_{01}}{\sqrt{2}} = \frac{2}{\sqrt{\pi}} \frac{x+y}{w_0^2} \exp\left[-\frac{x^2+y^2}{w_0^2}\right], \quad (3.5a)$$

$$B_2(x,y) = \frac{A_{10}-A_{01}}{\sqrt{2}} = \frac{2}{\sqrt{\pi}} \frac{x-y}{w_0^2} \exp\left[-\frac{x^2+y^2}{w_0^2}\right]. \quad (3.5b)$$

In the following we will call TEM_{10} the mode B_1 and TEM_{01} the mode B_2 . (c) The two doughnut modes with positive and negative helicity for which $f_{10}^{st}=f^{st}$, $f_{01}^{st}=\pm if^{st}$. The stationary field is $F^{st}=DGH_{\pm}f^{st}$, with the doughnut modes DGH_{\pm} defined by

$$DGH_{+}(x,y) = \frac{A_{10}+iA_{01}}{\sqrt{2}} = \frac{2}{\sqrt{\pi}} \frac{x+iy}{w_0^2} \exp\left[-\frac{x^2+y^2}{w_0^2}\right], \quad (3.6a)$$

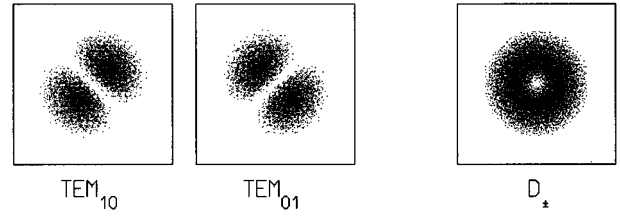


FIG. 2. Intensity distribution of TEM_{10} , TEM_{01} , and doughnut modes in the transverse plane.

$$DGH_{-}(x,y) = \frac{A_{10}-iA_{01}}{\sqrt{2}} = \frac{2}{\sqrt{\pi}} \frac{x-iy}{w_0^2} \exp\left[-\frac{x^2+y^2}{w_0^2}\right]. \quad (3.6b)$$

The transverse intensity distributions of modes TEM_{10} and TEM_{01} and doughnut modes are shown in Fig. 2.

The field intensity $|f^{st}|^2$ of the stationary solutions can be calculated for any value of the pump parameters μ and l_A using the integral equation

$$1 = \mu \int_{-l_A/2}^{l_A/2} dx \int_{-l_A/2}^{l_A/2} dy \frac{|g(x,y)|^2}{1+|g(x,y)|^2|f^{st}|^2}, \quad (3.7)$$

where $g(x,y)$ denotes anyone of the possible mode functions A_{10} , A_{01} , $B_{1,2}$, and DGH_{\pm} .

The laser threshold μ_{thr} is obtained by putting $|f^{st}|^2=0$ in Eq. (3.7). It turns out to be the same for the three kinds of stationary solutions and it depends only on the normalized size of the active region $\psi=l_A/w_0$

$$\mu_{thr} = \left[\frac{2}{\pi} J_0\left(\frac{\psi}{\sqrt{2}}\right) J_2\left(\frac{\psi}{\sqrt{2}}\right) \right]^{-1}, \quad (3.8)$$

with

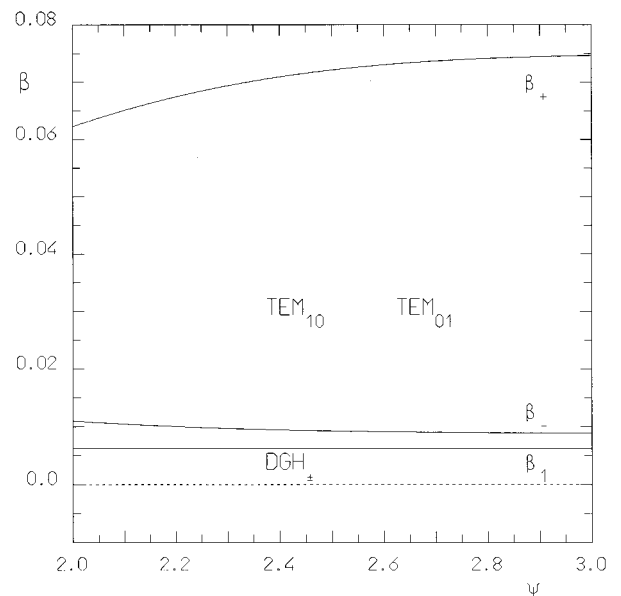


FIG. 3. Stability domains of the solutions DGH_{\pm} , TEM_{10} , and TEM_{01} in the plane (ψ, β) . The dashed line represents laser threshold.

$$J_n(z) = \int_{-z}^z dx x^n e^{-x^2}. \quad (3.9)$$

$$\beta = \frac{\mu}{\mu_{thr}} - 1 = \frac{I - I_{thr}}{I_{thr} - I_0}, \quad (3.10)$$

As the three kinds of stationary solutions have the same threshold, what determines which of them is the actual mode of emission of the laser is their stability against noise induced fluctuations. We have performed a standard linear stability analysis of the three stationary solutions. In order to simplify the calculations we have considered the limit of laser close to threshold, in which the substitution $(1 + |F|^2)^{-1} \rightarrow 1 - |F|^2$ allows for solving analytically the integrals which appear in the linearized equations. In this limit it is convenient to introduce the normalized pump parameter

which represents the excess of injected current relative to threshold. The condition of laser very close to threshold amounts to assuming $\beta \ll 1$, which in turn implies $|f^{st}|^2 \propto \beta$.

It was demonstrated in [16] that only the two modes B_1 (TEM₁₀) and B_2 (TEM₀₁) and the two doughnut modes DGH_{\pm} can be stable. For fixed values of α , τ_p/τ_r and ψ , the boundaries of the stability domains for the two kinds of stationary solutions are assigned by the following critical values of β [16]:

$$\beta_1 = \frac{\tau_p}{\tau_r} \frac{1}{\alpha^2}, \quad (3.11)$$

$$\beta_{\pm} = \frac{\tau_p}{\tau_r} \frac{H(1 + \alpha^2) + 2(1 - 2H) \pm \sqrt{H^2(1 + \alpha^2)^2 - 4\alpha^2(1 - 2H)^2}}{2(1 - H)^2(1 + \alpha^2)}, \quad (3.12)$$

with

$$H(\psi) = \frac{J_0(\psi)J_4(\psi) - J_2(\psi)^2}{J_0(\psi)J_4(\psi) + 3J_2(\psi)^2}. \quad (3.13)$$

By increasing β we meet the following sequence of stationary and dynamical regimes: (a) $0 < \beta < \beta_1$: the two doughnut modes are stable, (b) $\beta_1 < \beta < \beta_-$: the two doughnut modes beat at frequency

$$\omega_1 = \frac{1}{\tau_r \alpha}, \quad (3.14)$$

(c) $\beta_- < \beta < \beta_+$: modes TEM₁₀ and TEM₀₁ are stable, (d) $\beta > \beta_+$: modes TEM₁₀ and TEM₀₁ beat at frequency

$$\omega_2 = \frac{1}{\tau_r} \frac{[-2(1 - 2H)^2 + H^2(1 + \alpha^2) + H\sqrt{H^2(1 + \alpha^2)^2 - 4\alpha^2(1 - 2H)^2}]^{1/2}}{\sqrt{2}(1 - H)}. \quad (3.15)$$

Figure 3 shows the stability domains of the doughnut modes and of modes TEM₁₀ and TEM₀₁ in the (ψ, β) plane for $\alpha = 4$ and $\tau_p = 0.1\tau_r$.

It is worth noting that the width of the two bistability domains is proportional to the ratio τ_p/τ_r : in order to have significant bistability domains above threshold, the photon lifetime τ_p must not be too much smaller than the carrier lifetime τ_r . This requires very high mirror reflectivity ($R > 0.995$).

IV. OPTICAL SWITCHING OF MODES TEM₁₀ AND TEM₀₁

Since the bistability domain of doughnut modes is very small, in the following we will consider only the case in which the two bistable states of the VCSELs are modes TEM₁₀ and TEM₀₁. In this section we will investigate the conditions for switching from one to the other mode by means of an injected signal.

We assume that the injected field is a Gaussian (both in

time and in space) pulse of temporal width σ and spatial width η centered at a point (x_0, y_0) in the transverse plane and at time $t = 2\sigma$

$$F_{inj}(x, y, t) = \sqrt{P} \left[\frac{2}{\pi} \right]^{1/4} \exp \left[- \frac{(t - 2\sigma)^2}{\sigma^2} \right] \left[\frac{2}{\pi} \right]^{1/2} \times \frac{1}{\eta} \exp \left[- \frac{(x - x_0)^2 + (y - y_0)^2}{\eta^2} \right]. \quad (4.1)$$

The total injected energy is

$$E = \int_{-\infty}^{\infty} dx \int_{-\infty}^{\infty} dy \int_{-\infty}^{\infty} dt F_{inj}^2 = \sigma P, \quad (4.2)$$

where P is the maximum normalized injected power. The dynamical equations of the laser with injected signal, neglecting carrier diffusion, are then

$$\frac{dg_1}{dt} = -i\Delta\omega g_1 + \frac{1}{\tau_p} y_1(t) - \frac{1}{\tau_p} (1-i\alpha) \times \left[g_1 - \int_{-\infty}^{\infty} dx \int_{-\infty}^{\infty} dy B_1 DF \right], \quad (4.3a)$$

$$\frac{dg_2}{dt} = -i\Delta\omega g_2 + \frac{1}{\tau_p} y_2(t) - \frac{1}{\tau_p} (1-i\alpha) \times \left[g_2 - \int_{-\infty}^{\infty} dx \int_{-\infty}^{\infty} dy B_2 DF \right], \quad (4.3b)$$

$$\frac{\partial D}{\partial t} = -\frac{1}{\tau_r} [D(1+|F|^2) - \chi(x,y)], \quad (4.3c)$$

with

$$F(x,y,t) = B_1(x,y)g_1(t) + B_2(x,y)g_2(t) \quad (4.4)$$

and

$$y_{1,2}(t) = \frac{1}{\sqrt{T}} \int_{-\infty}^{\infty} dx \int_{-\infty}^{\infty} dy B_{1,2} F_{inj}. \quad (4.5)$$

Since in this section we deal only with modes B_1 and B_2 , the electric field has been expressed in terms of these modes. The presence of the injected field has two consequences. First, the source terms y_1 and y_2 , which represent the projections of the injected field over modes B_1 and B_2 , have been added in the equation for modal amplitudes. The field F now represents the total intracavity field. The normalization of the injected field amplitudes to \sqrt{T} makes the coupling coefficient equal to the photon decay rate $1/\tau_p$. The second consequence is the introduction of the parameter $\Delta\omega$, which represents the frequency detuning between the laser and the injected field $\omega_{laser} - \omega_{inj}$.

Let us assume that the VCSEL is emitting mode TEM_{10} (B_1), and we want to cause switching to mode TEM_{01} (B_2). Then the injection point (x_0, y_0) and the beam waist η must be chosen in such a way to maximize the projection onto mode TEM_{01} (y_2) and minimize that onto mode TEM_{10} (y_1). It is found that this occurs when $x_0 = -y_0 = \sqrt{3/8}w_0$ and $\eta = w_0/\sqrt{2}$. With this choice of the injection parameters we have $y_1 = 0$ and

$$y_2(t) \approx 0.59 \left(\frac{P}{T} \right)^{1/2} \exp \left[-\frac{(t-2\sigma)^2}{\sigma^2} \right]. \quad (4.6)$$

Taking into account that the stationary power transmitted outside the cavity is $P_0 = |g_1^{st}|^2 T$, the above equation can be written as

$$y_2(t) \approx 0.59 \left(\frac{P}{P_0} \right)^{1/2} |g_1^{st}| \exp \left[-\frac{(t-2\sigma)^2}{\sigma^2} \right], \quad (4.7)$$

which allows us to express the injected amplitude in terms of the adimensional ratio P/P_0 of the injected and emitted powers.

The detuning parameter $\Delta\omega$ plays a crucial role in the switching process. If $\Delta\omega$ is too small, switching turns out to

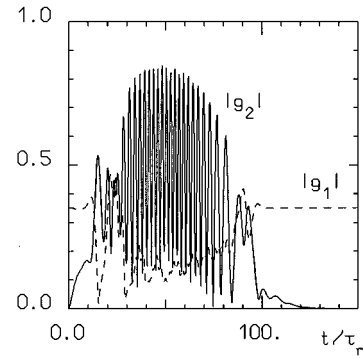


FIG. 4. Undamped oscillations of the TEM_{10} and TEM_{01} modes under injection of a high-energy pulse with $P=0.30P_0$ and $\sigma=25\tau_r$. The initial relative phase of injected and laser fields is $3\pi/4$. The other parameters are $\beta=0.0363$, $\tau_p=0.1\tau_r$, $\alpha=4$, and $\psi=2$. The dashed line represents the amplitude of mode TEM_{10} and the solid line that of mode TEM_{01} .

be very sensitive to the injection parameters, namely, the amplitude and duration of the injected pulse and its phase relative to the cavity field. Conversely, if $\Delta\omega$ is too large, switching becomes insensitive to the pulse duration and phase, but its threshold becomes very high.

Let us first examine the laser behavior in the case $\Delta\omega=0$. If the pulse is long and strong enough to cause an energy transfer that brings the laser to the upper unstable region of Fig. 3 the two competitive modes develop oscilla-

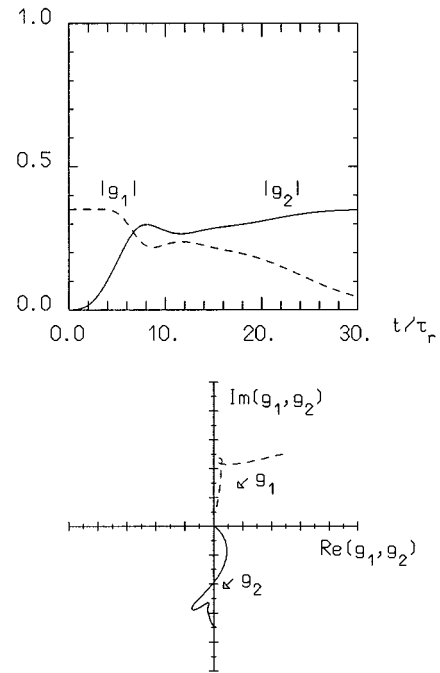


FIG. 5. Behavior of the laser modes amplitudes upon injection of a low-energy pulse with $P=0.001P_0$ and $\sigma=2\tau_r$. The other parameters are the same as in Fig. 4. An initial phase difference of $\pi/4$ is assumed between the injected and laser fields. In the top and bottom figures are shown, respectively, the mode amplitudes as a function of time and their evolution in the complex plane: switching takes place.

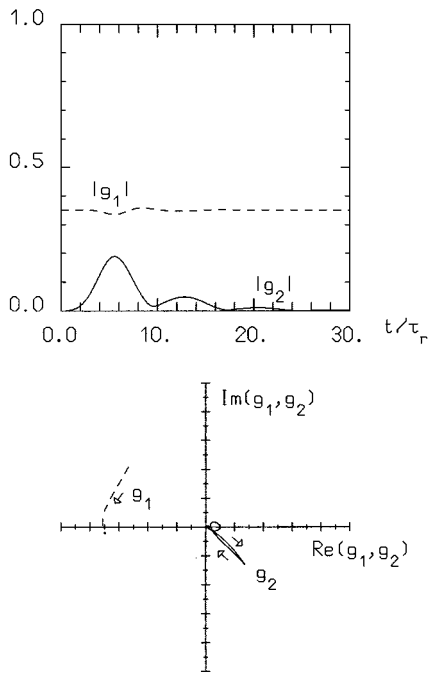


FIG. 6. Same as Fig. 5 but here an initial phase difference of $3\pi/4$ is assumed between the injected and laser fields. Switching does not take place.

tions (Fig. 4), and it becomes impossible to control which of the two will finally dominate. These oscillations can be avoided only by reducing the energy transfer to the system to the minimum value which is necessary to obtain switching; in principle this can be accomplished by injecting, for a short time, a pulse of low power. Unfortunately our simulation shows that in this case it becomes necessary to control the pulse phase. Figure 5 and Fig. 6 show the evolution of the two amplitudes g_1 and g_2 for injected pulses with the same amplitude and duration, but different phases: switching occurs in the case of Fig. 5 and it does not in the case of Fig. 6.

The introduction of a small detuning $\Delta\omega$ between the injected pulse and the cavity field has both the positive consequences of reducing the energy transfer to the system and eliminating the switching dependence on the phase. As one can see in Fig. 7, in the complex plane the effect of the detuned injected field is causing a relative rotation of the amplitudes g_1 and g_2 . To eliminate completely any influence on the switching process from the initial relative phase it is necessary that the pulse is long enough that during injection g_2 rotates at least 3 to 4 times around g_1 (Fig. 7); since the number of rotations can be roughly estimated to be $2\sigma\Delta\omega/2\pi$, the minimum pulse length is given by $\sigma \approx 3 \div 4\pi/\Delta\omega$. An unavoidable drawback is that the minimum power which must be injected to have switching increases, as shown in Fig. 8, where the ratio of switching power P_{sw} to the stationary power P_0 is plotted as a function of $\Delta\omega$. Yet, if $\Delta\omega \approx \tau_r^{-1}$ the switching power P_{sw} is still low: for instance, in the case of Fig. 7, $\Delta\omega = 3\tau_r^{-1}$, $\sigma = 6\tau_r$, and $P_{sw} \approx 0.28P_0$. Then, assuming $\tau_r = 0.2 \times 10^{-9}$ s and $P_0 = 0.1$ mW, the switching energy is $E_{sw} = \sigma P_{sw} \approx 30$ fJ. The whole switching process takes about 6 ns.

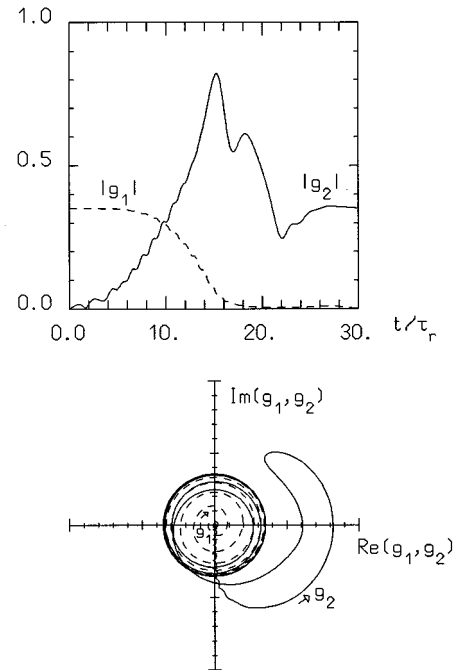


FIG. 7. Behavior of laser mode amplitudes upon injection of a pulse with $P = 0.30P_0$ and $\sigma = 6\tau_r$; a detuning $\Delta\omega = 3\tau_r^{-1}$ is assumed between the injected and laser fields. The other parameters are the same as in Figs. 4–6.

V. LOGIC GATES

Having demonstrated the feasibility of optical switching between modes TEM_{10} and TEM_{01} in a VCSEL with a square-shaped active region, we are now ready to apply this result to the realization of optical logic gates.

The logic gates most commonly used are the NOT, the OR, the AND, the NOR, and the NAND. Among these only the NOR and the NAND are fundamental, in the sense that combining a certain number of NOR or NAND gates it is possible to build any other logic gate.

A NOR gate can be realized as follows: two input beams (I_1, I_2) are injected in correspondence with the two peaks of one mode, say mode TEM_{01} ; the detector which measures the output (O) and a reset beam (Re) are placed on the other diagonal of the square (Fig. 9). Both the individual input

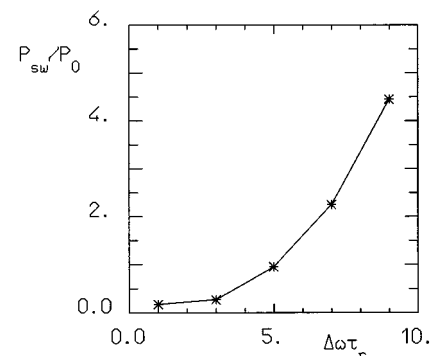


FIG. 8. Variation of the laser switching threshold P_{sw}/P_0 with increasing detuning, for an injected pulse with duration $\sigma = 6\tau_r$.

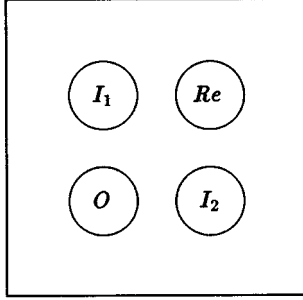


FIG. 9. Scheme of the logic gate NOR. I_1 and I_2 are the input beams, O is the output and Re is the reset beam.

beams and the reset beam have sufficient intensity to cause switching from one to the other mode.

We assign the value “1” to each of the inputs I_1 and I_2 when they are “on” and “0” when they are “off.” The detector measures “0” (no intensity) if the laser emits mode TEM_{01} and “1” (finite intensity) if the laser emits mode TEM_{10} . The reset beam, which is injected at the beginning of each operation, is necessary to ensure that initially the laser emits mode TEM_{10} . Then, if no beam is sent to any of the two inputs (i.e., $I_1=I_2=“0”$) the output is “1”; in all other cases the laser switches to mode 0 and the output is “0”; hence, the system works as a NOR gate.

Figure 10 shows the time evolution of mode intensities in the case in which both input beams take the value “1.” The whole operation consists of various steps. (a) the reset beam is switched on (in this particular case we assume that the result of the previous operation was “0,” that is the laser was on mode TEM_{01}), (b) the reset beam is switched off and the laser reaches the TEM_{10} mode, (c) the two input beams are injected, one after the other, into the laser, (d) the injection of the input beams causes the switching to mode TEM_{01} , (e) the output is detected. In step (c) the time separation between the injected pulses, equal to 4σ , is necessary to reduce interference between them, that in special cases might prevent the laser from switching. Actually, even with

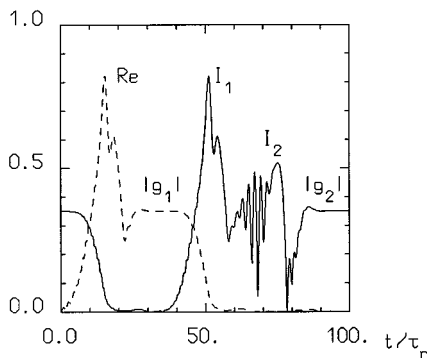


FIG. 10. Time behavior of the laser mode amplitudes during the sequence (a)–(e) described in the text, with the input beams assumed to be both “on.” Same parameters as in Fig. 7. The Gaussian pulses corresponding to the reset beam (Re) and to the two input beams (I_1, I_2) are centered at times $12 \tau_r$, $48 \tau_r$, and $72 \tau_r$, respectively.

this delay, the response of the laser to the second pulse (I_2) is very different from that to the first one (I_1). The whole logic process (a)–(e) takes about $100\tau_r$.

An OR gate is immediately obtained from the NOR simply by locating the output in the other diagonal; a NOT gate can also be obtained from the NOR one, by simply eliminating one of the input signals.

For the AND and NAND gates the situation is more complicated, because the laser must switch only when both input beams are “on.” One can think of injecting simultaneously the two beams, setting the intensity of the “on” signal to a value in the range between the switching threshold and one half of it; unfortunately the two pulses, depending on their detuning and phase difference, can interfere and cancel each other. It becomes therefore necessary to control the interference conditions or change globally the whole device design: investigations are going on in both these directions.

We observe that the scheme proposed here for logic gates can work only when the two stable states of the laser do not overlap in the transverse plane, as in the case of modes TEM_{10} and TEM_{01} . In this way the two output levels are associated with two intensity levels of the emitted field in a particular point.

The situation in which the two bistable states are the doughnut modes is less convenient for applications, because in this case the two outputs have the same intensity levels and they can be discriminated only by means of phase-sensitive techniques [13]. We note also that the kind of logic gate we propose has gain, and therefore allows for cascading.

VI. EFFECTS OF CARRIER DIFFUSION

All the previous results have been obtained assuming $l_D \ll w_0$, i.e., neglecting the effects of carrier diffusion in the transverse plane. As soon as the diffusion term in Eq. (2.8b) is taken into account, an analytic study of stationary solutions of Eqs. (2.8a) and of their stability becomes impossible. However, we can determine the shape of carrier distribution in the transverse plane below laser threshold and hence the value of laser threshold μ_{thr} , which differs from the one obtained neglecting diffusion. In the absence of diffusion and below threshold the profile of the carrier density coincides with the function $\chi(x, y)$; carrier diffusion smooths the contours of $\chi(x, y)$. The stationary profile of carrier density D when the electric field is equal to zero, is governed, according to Eq. (2.8b), by the equation

$$0 = D(x, y) - \chi(x, y) - l_D^2 \nabla_{\perp}^2 D(x, y), \quad (6.1)$$

with $\chi(x, y)$ given by Eq. (2.11) with $\mu_0 = 0$. It is convenient to introduce the Fourier transforms $\tilde{D}(u, v)$ and $\tilde{\chi}(u, v)$ defined by

$$D(x, y) = \int_{-\infty}^{\infty} du \int_{-\infty}^{\infty} dv \tilde{D}(u, v) \exp \left[i \frac{2\pi}{l_A} (ux + vy) \right] \quad (6.2)$$

and

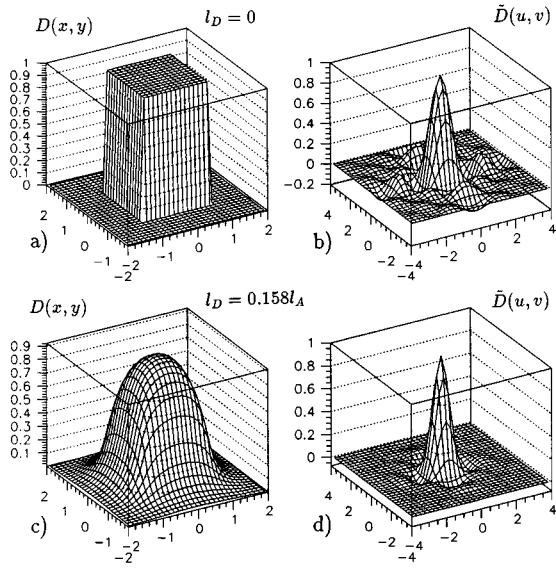


FIG. 11. Transverse profile of stationary carrier density $D(x,y)$ and of its Fourier transform $\tilde{D}(u,v)$ in absence of carrier diffusion (a) and (b), and for $l_D=0.158l_A$ (c) and (d).

$$\chi(x,y) = \int_{-\infty}^{\infty} du \int_{-\infty}^{\infty} dv \tilde{\chi}(u,v) \exp\left[i \frac{2\pi}{l_A}(ux+vy)\right]. \quad (6.3)$$

The Fourier transform of $\chi(x,y)$ is

$$\tilde{\chi}(u,v) = \mu \text{sinc}(u) \text{sinc}(v). \quad (6.4)$$

Then, from Eq. (6.1) we obtain

$$\tilde{D}(u,v) = \mu \frac{\text{sinc}(u) \text{sinc}(v)}{1 + (2\pi l_D/l_A)^2(u^2+v^2)} \quad (6.5)$$

and, taking into account the symmetry properties of $\tilde{D}(u,v)$, the stationary profile $D(x,y)$ is

$$D(x,y) = \mu \mathcal{D}(x,y) \quad (6.6)$$

with

$$\mathcal{D}(x,y) = \int_{-\infty}^{\infty} du \int_{-\infty}^{\infty} dv \tilde{D}(u,v) \cos\left[\frac{2\pi}{l_A}(ux+vy)\right]. \quad (6.7)$$

Figure 11 shows the stationary profiles of $D(x,y)$ below threshold and the corresponding Fourier transform $\tilde{D}(u,v)$ for $l_D=0$ [Figs. 11(a), 11(b)] and for $l_D=0.158l_A$ [Figs. 11(c), 11(d)]. The complementarity principle is evident: the more ‘‘localized’’ is $D(x,y)$ the less ‘‘localized’’ is $\tilde{D}(u,v)$.

The above results allow for the determination of the lasing threshold in the presence of carrier diffusion. The threshold is the same for the doughnuts, TEM_{10} and TEM_{01} modes and it is given by

$$1 = \mu_{thr} \int_{-\infty}^{\infty} dx \int_{-\infty}^{\infty} dy |A(x,y)|^2 \mathcal{D}(x,y), \quad (6.8)$$

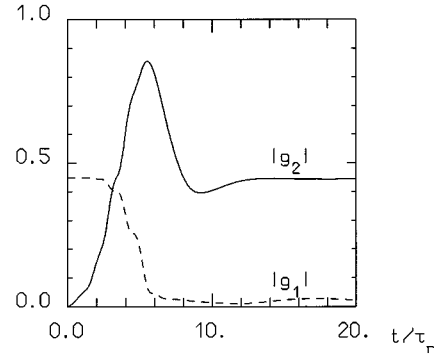


FIG. 12. Optical switching in presence of carrier diffusion. All the parameters are the same as in Fig. 7 apart from $l_D=0.158l_A$ and $\sigma=2\tau_r$.

where $A(x,y)$ is any of the functions DGH_+ , DGH_- , B_1 and B_2 . The value of μ_{thr} increases considerably with l_D . For instance, for $l_A=2w_0$, we have $\mu_{thr}=1.418$ for $l_D=0$ and $\mu_{thr}=1.728$ for $l_D=0.158l_A$. This fact is quite obvious: in the presence of carrier diffusion some carriers escape from the region occupied by the active modes and they do not participate any longer in laser emission.

Another important consequence of carrier diffusion is the enlargement of the stability domain for single mode stationary solutions TEM_{10} and TEM_{01} . In this case it is not possible to derive analytically the equations for the boundaries of the stability domains. The stability of stationary solutions was checked by numerical integration of the dynamical equations. For instance, in the absence of diffusion and with $\psi=2$, Fig. 3 shows that the stable range for the pump parameter β is $[0.011, 0.063]$. Numerical simulations with the same parameters and $l_D=0.158l_A$ show that now the solutions TEM_{10} and TEM_{01} are stable for β in the interval $[0.028, 0.225]$. Hence both lower and upper stability boundaries increase, in such a way that the stability domain becomes larger. We interpret this result in the following way: the instability mechanism for the single mode solutions TEM_{10} and TEM_{01} is spatial hole burning: in the presence of diffusion carriers are able to refill in part the holes burnt by the field, increasing the stability of the stationary solution.

Finally, we have found that for a fixed value of the ratio P/P_0 the switching time can be considerably smaller in the presence of diffusion. For instance, for the parameters of Fig. 7, the switching time was $\sigma_{sw}=5\tau_r$. With the same parameters and a diffusion coefficient $l_D=0.158l_A$, we found switching even for $\sigma=2\tau_r$, as shown in Fig. 12. This result can be explained considering that carriers move more easily from one configuration to the other in the presence of diffusion. However, it must be noted that, even if the injection time in the presence of diffusion is $2/5$ the injection time without diffusion, the ratio between the switching energy is about $2/3$. The reason is that, although the ratio P/P_0 is the same in the two cases, P_0 is larger in the case with diffusion, as can be seen from a comparison between the values of $|g_1^{st}|$ in Fig. 7 (≈ 0.35) and in Fig. 12 (≈ 0.45). Since the switching energy was about 30 fJ in absence of diffusion, we can estimate that diffusion reduces it to 20 fJ.

VII. CONCLUSIONS

We have demonstrated that VCSELs possess an especially interesting feature with respect to other kinds of lasers: the two Gauss-Hermite modes TEM_{10} and TEM_{01} can be both stable with an appropriate choice of the parameters and geometry. This property of VCSELs is the basis for applications to optical switching and logic gates. We have shown that the energy necessary to switch from one mode to the other can be as low as some tens fJ, while the switching time is on the order of a few ns. Switching is more reliable when a small detuning between the injected field and the laser field is present. In the presence of carrier diffusion in the transverse plane the threshold value for the injected current increases and the bistability domain of modes TEM_{10} and TEM_{01} becomes considerably larger. Moreover, if one keeps fixed the ratio of injected power P/P_0 , the switching energy is smaller, because the switching time is smaller. We have described in detail how, using this system, one can realize logic gates of the NOR, OR, and NOT type.

As discussed in Sec. II, in our model we neglect absorption coming from the passive parts of the VCSEL. Yet, since the main effect of absorption is to increase the laser threshold, it does not affect our rescaled parameter β . For instance, Fig. 13 shows the switching process with the same parameters as in Fig. 7 and a rather high absorption $\mu_0 = -1$. The behavior of mode amplitudes is indeed very similar to that of Fig. 7.

Finally, we want to point out some limitations of our model. First of all, we have assumed that the transverse modes of the VCSEL belonging to a family with the same value of $m+n$ are frequency degenerate. This is not the case in general, because the presence of any astigmatism in the laser makes the optical path different for modes with a different spatial profile. We need a large degree of transverse homogeneity in order to have perfectly degenerate modes. Asymmetries or strains of the material can break the fre-

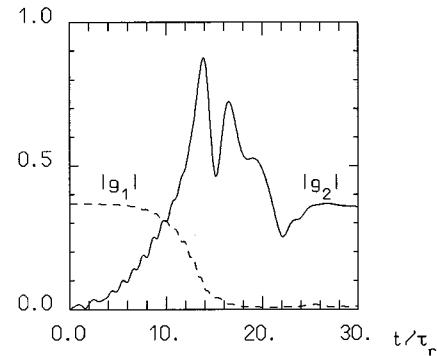


FIG. 13. Switching process with the same parameters as in Fig. 7, but with $\mu_0 = -1$, to take into account the effects of absorption.

quency degeneracy, and make bistability impossible [24]. We are confident that in a reasonable time VCSELs with a sufficient degree of homogeneity will be available.

Another difficulty is represented by the necessity of focusing the injected beam to a size on the order of a few microns, in order to excite only the desired mode. Spatial drifts of the injected field could also be detrimental for the reliability of the device.

Last but not least, a more realistic description should include light polarization, and we are working in that direction. In any case VCSELs, because of their particular properties and of the possibility of realizing cascaded configurations, seem to be interesting candidates for applications to information processing.

ACKNOWLEDGMENTS

We thank Professor J. McInerney and Dr. Hua Li for very helpful and stimulating discussions, and for disclosing to us their experimental results before publication. Work in the framework of the ESPRIT BR Project 7118 TONICS and of the NATO Collaborative Research Grant 921142.

-
- [1] L.A. Lugiato, Phys. Rep. **219**, 293 (1992).
 - [2] C.O. Weiss, Phys. Rep. **219**, 311 (1992).
 - [3] W.J. Firth, J. Mod. Opt. **37**, 151 (1990); G. D'Alessandro and W.J. Firth, Phys. Rev. Lett. **66**, 2597 (1991).
 - [4] J. Lega, J.V. Moloney, and A.C. Newell, Physica D **83**, 478 (1995).
 - [5] F.T. Arecchi, G. Giacomelli, P.L. Ramazza, and S. Residori, Phys. Rev. Lett. **65**, 2531 (1990); **67**, 3749 (1991).
 - [6] M. Kreuzer, W. Balzer, and T. Tschudi, Appl. Optics **29**, 579 (1990); R. Macdonald and H.J. Eichler, Opt. Commun. **89**, 289 (1992); B. Thuring, R. Neubecker, and T. Tschudi, *ibid.* **102**, 111 (1993); M. Tamburrini, M. Bonavita, S. Wabnitz, and E. Santamato, Opt. Lett. **18**, 855 (1993).
 - [7] S.A. Akhmanov, M.A. Vorontsov, V.Yu. Ivanov, A.V. Larichev, and N.I. Zheleznykh, J. Opt. Soc. Am. B **9**, 78 (1992); E. Pampaloni, S. Residori, P.L. Ramazza, and F.T. Arecchi, Phys. Rev. Lett. **74**, 258 (1995); **76**, 1063 (1996).
 - [8] G. Giusfredi, J.F. Valley, R. Pon, G. Khitrova, and H.M. Gibbs, J. Opt. Soc. Am. B **5**, 1181 (1988); A. Petrossian, M. Pinard, A. Maitre, J.Y. Courtois, and G. Grynberg, Europhys. Lett. **18**, 689 (1992); G. Grynberg, A. Maitre, and A. Petrossian, Phys. Rev. Lett. **72**, 2379 (1994); D. Leduc, M. Le Berre, E. Ressayre, and A. Tallet, Phys. Rev. A **53**, 1072 (1996).
 - [9] L.A. Lugiato, Chaos, Solitons Fractals **4**, 1251 (1994), introductory article to the special issue *Nonlinear Optical Structures, Patterns, Chaos*.
 - [10] M. Brambilla, F. Battipede, L.A. Lugiato, V. Penna, F. Prati, C. Tamm, and C.O. Weiss, Phys. Rev. A **43**, 5090 (1991).
 - [11] M. Brambilla, L.A. Lugiato, V. Penna, F. Prati, C. Tamm, and C.O. Weiss, Phys. Rev. A **43**, 5114 (1991).
 - [12] C. Tamm, Phys. Rev. A **38**, 5960 (1988).
 - [13] C.P. Smith, Y. Dihadja, C.O. Weiss, L.A. Lugiato, F. Prati, and P. Vanotti, Opt. Commun. **102**, 505 (1993).
 - [14] J.L. Jewell, J.P. Harbison, A. Scherer, Y.H. Lee, and L.T. Florez, IEEE J. Quantum Electron. **QE-27**, 1332 (1991).
 - [15] C.H. Henry, IEEE J. Quantum Electron. **QE-18**, 259 (1982).
 - [16] F. Prati, A. Tesei, L.A. Lugiato, and R.J. Horowicz, Chaos, Solitons Fractals **4**, 1637 (1994).

- [17] F. Prati, M. Travagnin, and L.A. Lugiato, *Opt. Lett.* **19**, 1991 (1994).
- [18] F. Prati, M. Brambilla, and L.A. Lugiato, *Riv. Nuovo Cimento* **17** (3), 1 (1994).
- [19] E.J. D'Angelo, E. Izaguirre, G.B. Mindlin, G. Huyet, L. Gil, and J.R. Tredicce, *Phys. Rev. Lett.* **68**, 3702 (1992).
- [20] C.J. Chang–Hasnain, M. Orenstein, A.C. Von Lehmen, L.T. Florez, J.P. Harbison, and N.G. Stoffel, *Appl. Phys. Lett.* **57**, 218 (1990).
- [21] C.J. Chang–Hasnain, J.P. Harbison, G. Hasnain, A.C. Von Lehmen, L.T. Florez, and N.G. Stoffel, *IEEE J. Quantum Electron.* **QE-27**, 1402 (1991).
- [22] C.J. Chang–Hasnain, Y.A. Wu, G.S. Li, G. Hasnain, K.D. Choquette, C. Caneau, and L.T. Florez, *Appl. Phys. Lett.* **63**, 1307 (1993).
- [23] K. Tai, Y. Lai, K.F. Huang, T.C. Huang, T.D. Lee, and C.C. Wu, *Appl. Phys. Lett.* **63**, 2624 (1993).
- [24] H. Li, T.L. Lucas, J. McInerney, and R.A. Morgan, *Chaos, Solitons Fractals* **4**, 1619 (1994).
- [25] F.B. de Coulstoun, G. Khitrova, V.A. Fedorov, T.R. Nelson, C. Lowry, T.M. Brennan, B.G. Hammons, and P.D. Maker, *Chaos, Solitons Fractals* **4**, 1575 (1994).
- [26] A.K. Jansen van Doorn, M.P. van Exter, and J.P. Woerdman, *Electron. Lett.* **30**, 1941 (1994).
- [27] P.D. Dapkus, N. Holonyak, Jr., R.D. Burnham, D.L. Kleune, J.W. Burd, K.L. Lawley, and R.E. Walline, *J. Appl. Phys.* **41**, 4194 (1970).